Petroleum Science xxx (xxxx) xxx

Contents lists available at ScienceDirect

Petroleum Science

journal homepage: www.keaipublishing.com/en/journals/petroleum-science

Original Paper

Molecular insights into the effects of representative organic molecules on spontaneous hydrate nucleation in oceanic sediments

Feng-Yi Mi [a,b], Zhong-Jin He [a,*], Jiang-Tao Pang [a], Othonas A. Moultos [c], Thijs J.H. Vlugt [c], Guo-Sheng Jiang [a], Fu-Long Ning [a]

[a] National Center for International Research on Deep Earth Drilling and Resource Development, Faculty of Engineering, China University of Geosciences, Wuhan, 430074, Hubei, China
[b] Key Laboratory of Solid Waste Treatment and Resource Reuse, Ministry of Education, Southwest University of Science and Technology, Mianyang, 621010, Sichuan, China
[c] Engineering Thermodynamics, Process & Energy Department, Faculty of Mechanical Engineering, Delft University of Technology, Leeghwaterstraat 39, Delft, 2628CB, Netherlands

ARTICLE INFO

Article history:
Received 6 September 2025
Received in revised form
30 November 2025
Accepted 9 February 2026
Available online xxx

Edited by Min Li

Keywords:
Methane hydrate
Molecular dynamics simulation
Hydrate formation
Montmorillonite clay
Organic molecules
NaCl solution

ABSTRACT

Knowledge of the effect of different organic molecules on spontaneous hydrate nucleation is crucial for understanding the formation of gas hydrates in marine reservoirs. Herein, microsecond MD simulations are conducted to investigate the spontaneous nucleation of CH_4 hydrates in oceanic sediments. The simulation results indicate that hydrate nucleation is influenced by the coupling effects of organic molecules, clay surfaces and salt ions, where organic molecules alter hydrate nucleation by modulating the diffusion fluctuation of CH_4 molecules via controlling the shape and size of CH_4 nanobubbles. Furthermore, CH_4 hydrates are primarily concentrated at a moderate distance away from the nanobubbles, with fewer hydrates located either close or at a more distant from the nanobubbles. In the region about 1.0 nm away from the nanobubbles, the hydrates become more unstable when closer to the nanobubbles, whereas hydrates have better stability when locating above 1.0 nm away from the nanobubbles. Different organic molecules exert distinct effects on spontaneous hydrate nucleation. Specifically, propanol adsorbed to the nanobubble surface kinetically promotes hydrate nucleation, exhibiting a distinct advantage over other organic molecules. These molecular insights expand the understanding of the formation of natural gas hydrate resources and help to effectively utilize this resource.

1. Introduction

In the context of sustainable development goals, the pursuit of clean energy sources has been a major objective worldwide. Clean energy not only addresses the ever-growing energy demands but also plays a crucial role in mitigating climate change by reducing greenhouse gas emissions. Natural gas hydrates have emerged as a promising alternative due to their abundant reserves, world-wide distribution, low CO_2 emissions and so on (Boswell, 2009; Haq, 1999; Koh, 2002). Natural gas hydrates, mainly CH_4 hydrates, are ice-like compounds formed under specific conditions of low temperature and high pressure, encapsulating CH_4 molecules in the hydrogen-bond network of water molecules (Mi et al., 2025a; Sloan ED, 2008). Notably, the carbon reserves within CH_4 hydrates are estimated to be more than twice of the total reserves of conventional fossil fuels, a figure that may increase substantially in the future (Milkov, 2004; Sloan, 2003). CH_4 hydrates are widespread in permafrost regions and marine sediments and hold the potential to revolutionize the global energy landscape (Makogon et al., 2007; Zhang et al., 2022, 2023). Numerous countries have dedicated substantial endeavors to extract CH_4 gas from CH_4 hydrates (Collett et al., 2011; Konno et al., 2017; Li et al., 2018). However, high costs, sand production and secondary hydrate formation hinder the commercialization of hydrate exploitation (Li et al., 2016; Ning et al., 2012). One important scientific issue worthy of further exploration is the formation mechanism CH_4 hydrate, particularly in the complex marine environments where

* Corresponding author.
E-mail address: hezhongjin@cug.edu.cn (Z.-J. He).
Peer review under the responsibility of China University of Petroleum (Beijing).

https://doi.org/10.1016/j.petsci.2026.02.012

organic matter abounds (Kvenvolden, 1995; Qin et al., 2022; Wang et al., 2019). Understanding how various organic molecules influence the formation of CH_4 hydrates in marine sediments is of paramount importance for efficiently harnessing this unconventional energy source.

Due to the vast expanse of the ocean, it contains many different organic compounds. These organic molecules wield a continuous influence on the formation and decomposition of CH_4 hydrates (Huang et al., 2024; Kvenvolden, 1993). Liu et al. (2021a, 2021b, 2021c) systematically investigated the formation process of gas hydrates in solutions of self-assembled colloids, acid-soluble organic matter, protein macromolecules and metabolic small molecules from the experiments level. Their findings showed that different organic molecules exhibit diverse effects on the formation of gas hydrates. Furthermore, some studies reported eco-friendly hydrate inhibitors derived from natural organic matter (Yun et al., 2023), including cellulose (Jia et al., 2022), natural product pectin (Xu et al., 2016), amino acids (Bavoh et al., 2019), and antifreeze proteins (Zeng et al., 2006). On the other hand, a large number of organic matter molecules are active in hydrate formations, with the organic matter content in hydrate-containing sediments in the Ulleung Basin soaring to levels of up to 10% (Kelleher et al., 2007; Lamorena et al., 2011; Saito and Suzuki, 2007; Wallmann et al., 2006). The coupling effect of sediments with organic matter further complicates hydrate formation (Mi et al., 2024d; Saito and Suzuki, 2007; Zhang et al., 2003). Lamorena et al. (2011) conducted experiments and observed that the induction time of CO_2 hydrate formation in sediment suspensions containing organic matter is approximately 7 times faster than that in suspensions devoid organic matter. The experimental results of Zhao et al. (2021) showcased a 92% reduction in the induction time for hydrate formation owing to the synergy of organic matter and clay minerals. Similarly, Liu et al. (2023a, 2023b) showed that clay minerals and organic matter can synergistically promote the formation kinetics of CO_2 hydrate by controlling the arrangement of water molecules. The experimental results of Park et al. (2014) demonstrate that the influence of organic matter on CO_2 hydrate phase equilibrium conditions can be retained or reduced in layered silicate suspensions. Kyung et al. (2015) observed that the combination of organic matter and mineral matter enhanced the nucleation kinetics of CO_2 hydrate, and pointed out that the type and amount of soil minerals and organic matter can affect CO_2 hydrate formation. However, the diversity of organic matter within experimental samples has obscured the microscopic mechanisms of its influence on hydrate formation. Over the past decade, molecular dynamics (MD) simulation has been rapidly developed in the field of hydrate formation, which allows us to obtain mechanisms and phenomena at the molecular scale that are difficult to be obtained through experimentation alone (Chen et al., 2023; Liao et al., 2023; Mi et al., 2023, 2025b; Walsh et al., 2009; Yan et al., 2023; Zhang et al., 2024). Ji et al. (2016, 2018) by using MD simulation found the inhibitory effect of humic acid and fatty acids in montmorillonite nanopores on the formation of CH_4 hydrate. Based on MD simulations, Fengyi et al. (2023) and Mi et al. (2024a) revealed that lignin and glucose molecules inhibit CH_4 hydrate formation by promoting CH_4 nanobubble formation and inhibiting CH_4 nanobubble decomposition.

However, the mechanism of how various organic matter molecules in hydrate-bearing sediments influence the spontaneous nucleation of CH_4 hydrates remains obscure. It is worth noting that the coupling effects of some geological factors in hydrate-bearing sediments, including organic molecules, salt ions and clay minerals, further complicate the nucleation process of CH_4 hydrates in marine sediments. However, the mechanism of the coupling effect on hydrate nucleation has not yet been systematically explored. Thus, this study performs microsecond MD simulation on the spontaneous nucleation of CH_4 hydrates from organo-clay salt solutions in clay nanopores, to reveal the influence mechanism of different organic molecules. This preliminary study into the microscopic mechanism of the effect of organic molecules on spontaneous hydrate nucleation can help to understand the formation of natural gas hydrate resources, and will catalyze more inventive research, particularly with regard to CH_4 hydrate exploitation, hydrate-based CO_2 sequestration and seawater desalination.

2. Simulation models and methods

Clay minerals are one typical component of hydrate-bearing sediments that can significantly change the kinetics and thermodynamics of hydrate formation (Liu et al., 2023c; Mi et al., 2024b; Ren et al., 2022, 2023; Wang et al., 2025; Zhu et al., 2024). The clay unit cell parameters were sourced from the American Mineral Crystal Database (Downs and Hall-Wallace, 2003). The molecular formula of the yielded Wyoming montmorillonite model used in this work is $Na_{0.75}(Si_{7.75}Al_{0.25})(Al_{3.5}Mg_{0.5})O_{20}(OH)_4$. The montmorillonite nanopore was created by stacking two identical montmorillonite plates with a defined pore size of 4.0 nm. Earlier MD research underscores the importance of pore size, as overly small pores hinder hydrate formation, while excessively large ones cannot exhibit the role of the clay surface (Mi et al., 2022a). A homogeneous solution containing 5352 H_2O molecules and 931 CH_4 molecules was placed in the montmorillonite nanopore. The water/gas ratio (~5.75:1) was the same as the ideal stoichiometry of a fully occupied sI-type hydrate. Such high gas supersaturation ensures that the rare event of spontaneous nucleation of CH_4 hydrate can be observed within a computationally feasible microsecond timescale in MD simulations, allowing for a comparison of the effects of different organic molecules under the same conditions. Sodium chloride ions with a salinity of 3.5 wt% were randomly placed into the homogeneous solution.

Hydrate-bearing sediments encompass various organic matter molecules, including *n*-alkanes, alcohols, aromatics, isoprenoids, fatty acids, and nitrogen source amino acids, each characterized by distinct functional groups. Six small organic molecules were selected, all sharing a common propyl skeleton structure but differing in their functional groups (methyl, hydroxyl, phenyl, double bond, carboxyl and amino), i.e., the butane, propanol, phenylpropane, pentene, butyric-acid and propylamine. The molecular structures of six small organic molecules are shown in Fig. S1. 50 small organic molecules were randomly inserted into the nanopore. A schematic representation of the final model is shown in Fig. 1. A control system without organic molecules was used for comparison. Therefore, MD simulation of seven different systems was performed, i.e., the systems of $MO_{No\text{-}organic}$, $MO_{Butyric\text{-}acid}$, $MO_{Propylamine}$, $MO_{Propanol}$, $MO_{Pentene}$, MO_{Butane} and $MO_{Phenylpropane}$. The specific number of molecules and ions in each system is shown in Table S1. The principles of the methods used in this study to analyze the data are provided in the Supporting Information. Hydrate nucleation is fundamentally a stochastic process. While a single, ultra-long 3.0 μs simulation performed for each system allows for the detailed observation of molecular mechanisms and some kinetically-driven trends, some quantitative metrics for hydrate nucleation, such as the induction time and hydrate cage numbers, may be different across independent runs. Nevertheless, this work focuses on the qualitative differences and the underlying molecular mechanisms that are consistently observed over these extended simulation timescales, rather than

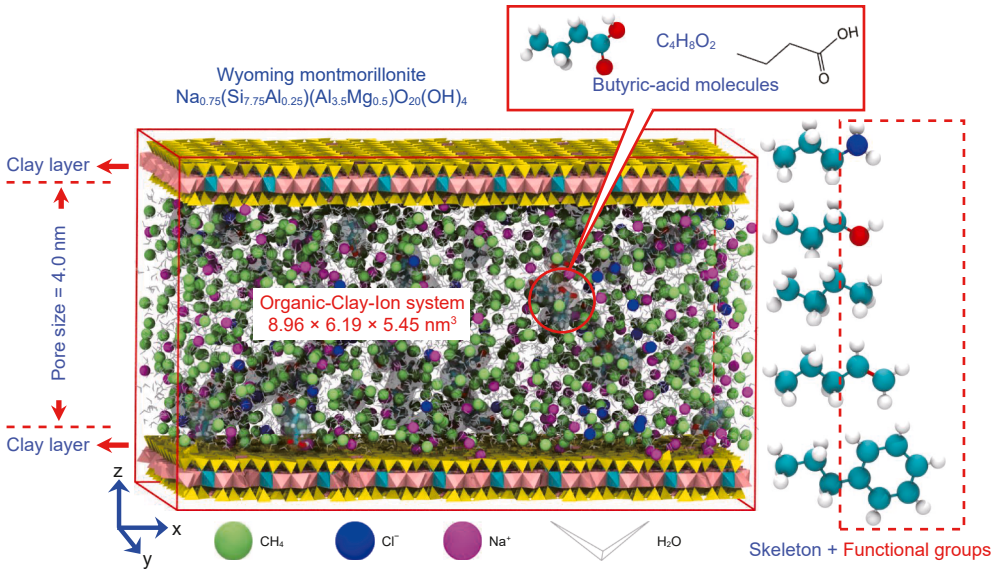

Fig. 1. A schematic representation of the simulation model. The molecular structures of the six small organic molecules are shown. Small organic molecules are displayed as cyan (C atom), red (O atom) blue (N atom) and white (H atom). Clay layers are displayed as polyhedral, i.e., yellow (Si atom), cyan (Mg atom) and pink (Al atom). Blue, magenta, and green balls represent Cl^-, Na^+, and CH_4, respectively.

some quantitative metrics for hydrate nucleation. Thus, only one simulation run has been performed for each system.

CH_4, H_2O, and the organic molecules were represented by the OPLS–UA model (Jorgensen et al., 1984), TIP4P–ice model (Abascal et al., 2005) and OPLS–AA force field (Jorgensen et al., 1996), respectively. Montmorillonite and ions were represented by the CLAYFF force field (Cygan et al., 2004), which has been widely used and well-validated in previous MD work (Fang et al., 2024; Li et al., 2022; Mi et al., 2024c). For the short-range nonbonded interactions, Lennard-Jones potentials with a cutoff distance of 1.0 nm were used. Long-range electrostatic interactions were treated using the particle mesh Ewald (PME) (Darden et al., 1993) within a Fourier space extending 1.2 nm. Periodic boundary conditions were assigned in *x*, *y*, and *z* directions, and the rigidity of water molecules was preserved via the SHAKE algorithm. The leap-frog integrator algorithm with a time step of 2.0 fs was used to integrate the equations. The detailed force field parameters for H_2O, CH_4, ions, montmorillonite, and organic molecules in the system are shown in Tables S2 and S3.

Three simulation stages were performed for each system: initially, energy minimization was performed to relax the initial configuration. Then, a 5 ns equilibration simulation was performed under the isothermal-isobaric (NPT) ensemble, with the temperature (250 K) and pressure (50 MPa) controlled by velocity-rescaling thermostat (Bussi et al., 2007) and Berendsen barostat (Berendsen et al., 1984), respectively. The condition of low temperature and high pressure accelerates hydrate formation and reduces computational cost (Mi et al., 2022b). Finally, an ultra-long 3.0 μs production simulation was carried out under the NPT ensemble, with temperature and pressure controlled by the Nosé-Hoover thermostat (Nosé, 1984) and Parrinello-Rahman barostat (Parrinello and Rahman, 1980), respectively. The pressure coupling was semi-isotropic, allowing independent fluctuations along the normal (*z*-dimension) and lateral (*xy*-dimensions) directions. All the MD simulations were performed utilizing the GROMACS package v.5.0.7 (Hess et al., 2008).

3. Results and discussions

3.1. Interplay between organic molecules, CH_4, H_2O, ions and clay surface

The interplay of small organic molecules, clay surfaces, CH_4, H_2O, and ions plays a critical role in altering the spontaneous nucleation of CH_4 hydrates. The MD simulations revealed two interfacial water layers near the montmorillonite surface (Fig. 2(a)). The first interfacial water layer exhibits a high-density peak (Figs. 2(a) and S2(a)–(g)). This can be attributed to an over-adsorption phenomenon, where H_2O molecules densely adhere to the montmorillonite surface, collectively forming a tightly packed interfacial layer. In contrast, the second interfacial water layer shows a lower density peak than the first one. This discrepancy in density arises from the hydration shell formed as ions are hydrated and adsorb to the montmorillonite surface (Figs. 2(a) and S2(a)–(g)). Most of the ions adsorb on the montmorillonite surface to form an interfacial ion layer (Figs. 2(a) and S3(a)–(g)). Na^+ ions swiftly adsorb on the montmorillonite surface to compensate for its negative charges. In stark contrast, CH_4 molecules predominantly locate in the middle region of the montmorillonite nanopores, as observed in Figs. 2(a) and S4(a)–(g). This distribution effectively separates CH_4 molecules from the clay surface by the interfacial water and ion layers, rendering them less prone to adsorption on the montmorillonite surface. This phenomenon is also observed in $MO_{No\text{-}organic}$, $MO_{Butyric\text{-}acid}$, $MO_{Propylamine}$, $MO_{Pentene}$, MO_{Butane} and $MO_{Phenylpropane}$ systems (Fig. S5(a)–(g)). All six types of organic molecules considered in this work mostly locate in the middle region of the nanopores (Figs. 2(a) and S6(a)–(g)). Even in the presence of functional groups (such as hydroxyl, carboxyl and amino) capable of forming hydrogen bonds with the clay surface, these small organic molecules still encounter the physical barrier posed by the interfacial water and ion layers, which effectively prevents their direct interaction with the clay surface (Fig. S5(a)–(g)).

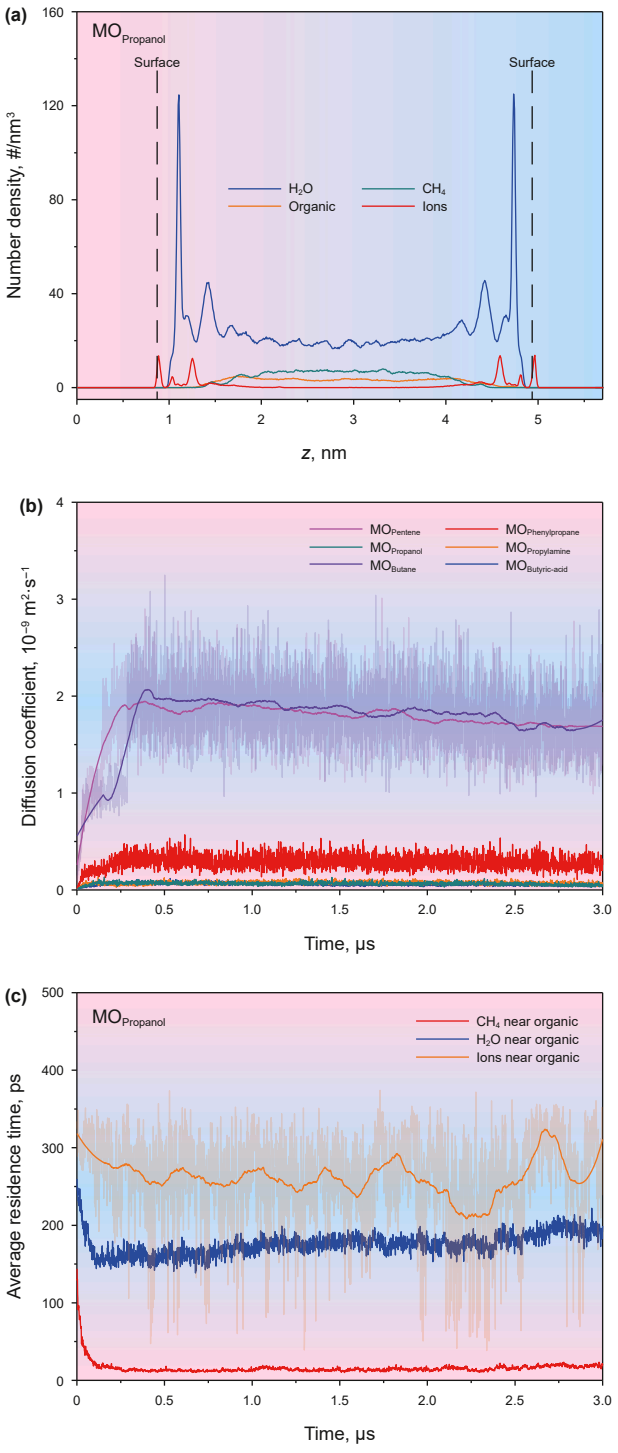

Fig. 2. **(a)** Number density distribution of H_2O, CH_4, organic molecules, and ions along the surface normal direction (z-axis) in the $MO_{Propanol}$ system over the 2.5–3.0 μs. **(b)** Evolution of the diffusion coefficient (k_{DC}) for six small organic molecules during hydrate formation, and **(c)** the average residence timae (τ_{Res}) for CH_4, H_2O and ions near small organic molecules in the $MO_{Propanol}$ system. τ_{Res} and k_{DC} are calculated over an interval of 1 ns, i.e., for each ns. We smoothed the curves in (b)–(c) with large jumps by running block average and then blurred the original curves.

Differences arise in the diffusion of these six types of small organic molecules in the middle region of the nanopores. The diffusion coefficients (k_{DC}) of the organic molecules during hydrate formation are shown in Fig. 2(b). Notably, pentene and butane molecules exhibit a swift increase in their k_{DC} values at the beginning of the simulation, maintaining a high plateau during the simulation period of 0.5–3.0 μs (Fig. 2(b)). This behavior is ascribed to the weak interaction between their functional groups (methyl and double bond) and H_2O molecules. Consequently, pentene and butane are essentially hydrophobic, enabling them to dissolve into CH_4 nanobubbles and contribute to the formation of mixed nanobubbles (Fig. S6(d)–(e)). Organic molecules in the gas phase diffuse faster compared to those in the liquid phase. Conversely, these hydrophilic functional groups (hydroxyl, carboxyl and amino) of propanol, propylamine and butyric-acid molecules can form hydrogen bonds with H_2O molecules in solution. These hydrophilic organic molecules tend to be distributed along the surfaces of CH_4 nanobubbles, i.e., the gas–liquid interface (Fig. S6(a)–(c)). Therefore, hydrophilic organic molecules generally exhibit slower diffusion during hydrate formation (Fig. 2(b)). In particular, the k_{DC} value of phenylpropane molecules is between that of the hydrophilic and hydrophobic organic molecules (Fig. 2(b)). A noteworthy observation is that, although inherently hydrophobic, phenylpropane molecules preferentially accumulate at the gas–liquid interface (Fig. S6(f)) rather than dissolving into the CH_4 nanobubble. This behavior may be due to the fact that inserting the large and rigid benzene ring into the densely packed nanobubble is energetically unfavorable due to the steric hindrance, consistent with previous studies (Fengyi et al., 2023; He et al., 2022). To gain further insight into the influence of organic molecules on their surroundings, we evaluated the residence time (τ_{Res}) of CH_4, H_2O, and ions close to these molecules. Based on the radial distribution function between the organic molecules and CH_4, H_2O and ions (Fig. S7(a)–(f)), an average cutoff distance of 0.4 nm is applied. It is observed that the τ_{Res} values for CH_4 and H_2O molecules decrease rapidly, eventually converging to 20 and 190 ps, respectively (Fig. 2(c)). This trend aligns with the behavior of the butane, phenylpropane, pentene, butyric-acid, and propylamine molecules (Fig. S8(a)–(f)). In the last stage of the simulation, it is found that the τ_{Res} value of ions around propanol molecules is the largest, followed by H_2O molecules and finally CH_4 molecules (Fig. 2(c)). This indicates that propanol molecules bind surrounding ions and H_2O molecules while exerting a relatively weak interaction with CH_4 molecules. The weaker the binding force of organic molecules to H_2O molecules, the more favorable the conditions for hydrate nucleation. Conversely, a stronger binding of organic molecules with ions tends to facilitate hydrate nucleation.

3.2. Spontaneous nucleation of CH_4 hydrate from organoclay salt solution in clay nanopore

In organo-clay salt solutions, the spontaneous nucleation of CH_4 hydrates is influenced by a coupling of organic molecules, clay surfaces, and salt ions. The spontaneous nucleation processes of CH_4 hydrate in the $MO_{Propanol}$ system are illustrated in Fig. 3(a)–(i). At the beginning of the simulation, clay surfaces exhibit a distinct affinity for ions while simultaneously repelling CH_4 and organic molecules; CH_4 molecules quickly form several nanobubbles; spontaneous nucleation of CH_4 hydrate forms sporadic 5^{12} and $5^{12}6^2$ cages (Fig. 3(a) and (b)). As the simulation proceeds, CH_4 nanobubbles gradually merge into a large spherical nanobubble (Fig. 3(c), (d) and (g)). The growth of hydrate cages occurs with the continued spontaneous nucleation of CH_4 hydrates, ultimately leading to the formation of CH_4 hydrate clusters (Fig. 3(c) and (d)). Moreover, the CH_4 nanobubble changes in shape from spherical to cylindrical during the simulation period of 1.24–1.25 μs, and the shape of the CH_4 nanobubble remains cylindrical in subsequent simulations (Fig. S9(a)–(d)). In the later stages of the simulation, the shape of the CH_4 nanobubble is spherical in the system without

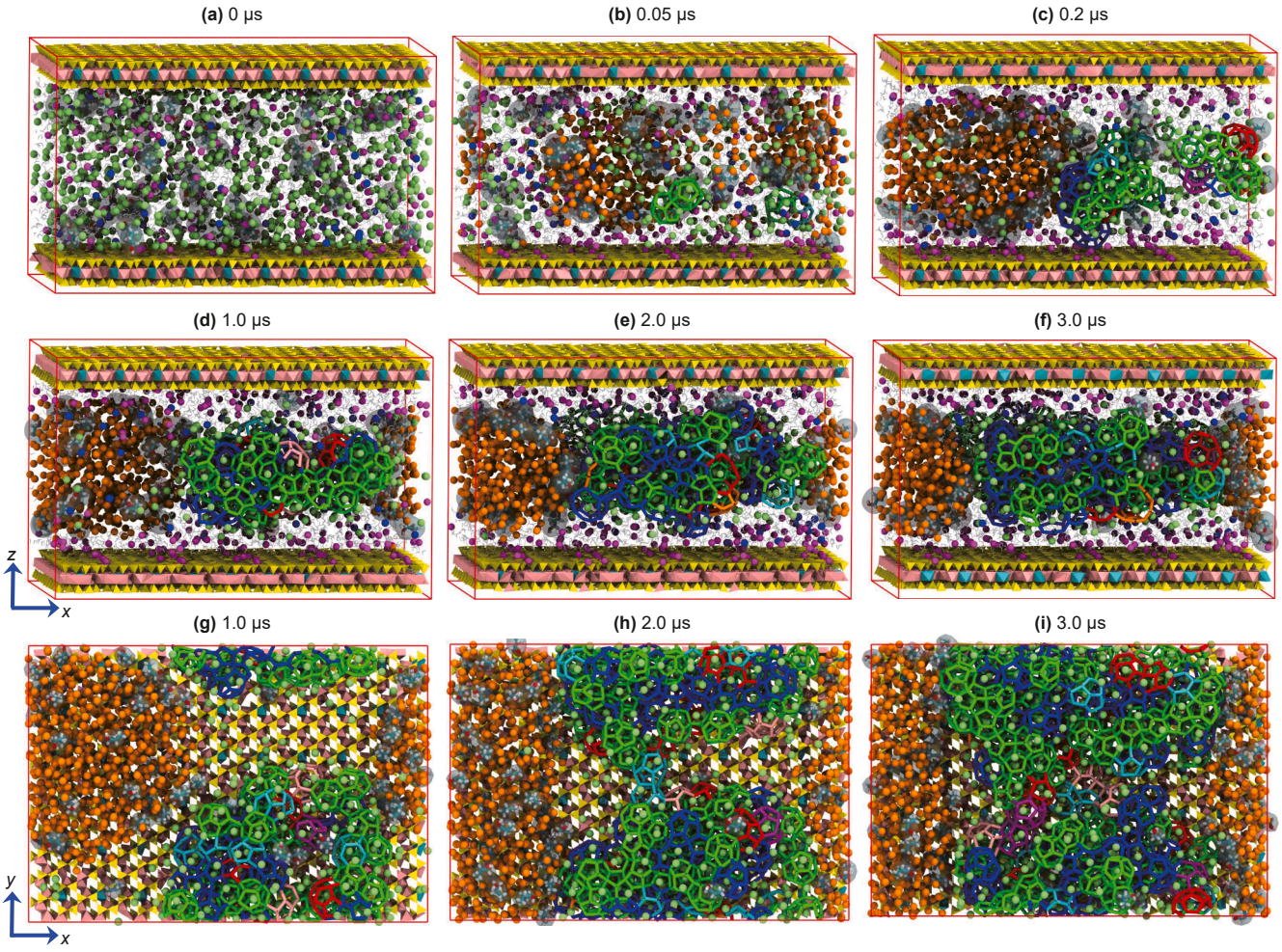

Fig. 3. Spontaneous nucleation processes of CH_4 hydrate from organoclay salt solutions for the **(a)**–**(f)** $MO_{Propanol}$ system. Bottom panels **(g)**–**(i)** highlight the distribution of CH_4 hydrate cages, small organic molecules, and CH_4 nanobubble. Organic molecules are displayed as cyan (C atom), red (O atom), blue (N atom), and white (H atom). Clay layers are displayed as polyhedral, i.e., yellow (Si atom), cyan (Mg atom) and pink (Al atom). Blue, magenta, orange, and green balls represent Cl^-, Na^+, CH_4 in nanobubble and CH_4 in solution, respectively. Hydrate cages are shown as sticks in various colors (green for 5^{12}, blue for $5^{12}6^2$, red for $5^{12}6^3$, orange for $5^{12}6^4$, cyan for $4^15^{10}6^2$, purple for $4^15^{10}6^3$ and pink for $4^15^{10}6^4$).

organic molecules, whereas the shape of the CH_4 nanobubbles is cylindrical in the system containing organic molecules (Figs. 3(h)–(i) and S10(a)–(g)). Several hydrate clusters converge to a large hydrate solid, predominantly distributed in the middle region of the nanopore (Fig. 3(e) and (f)). All organic molecules are mainly distributed inside or on the surface of CH_4 nanobubbles (Fig. S10(a)–(g)). To provide a more comprehensive and insightful perspective on these spontaneous nucleation processes of CH_4 hydrates from organoclay salt solutions, visualizations of the MD simulations are provided as Supporting Information for all seven systems in Videos S1–S7.

Supplementary video related to this article can be found at in the Supplementary Information https://doi.org/10.1016/j.petsci.2026.02.012.

Organic molecules alter the spontaneous nucleation of CH_4 hydrates by modulating the diffusion fluctuations for CH_4 molecules via controlling the shape and size of CH_4 nanobubbles. Organic molecules may promote the shape transformation of CH_4 nanobubbles from spherical to cylindrical. To reveal the effect of organic molecules on the fluctuation of CH_4 molecules, all CH_4 molecules in the system are divided into three types, namely near organic molecules, in the nanobubbles, and in the solution (Fig. S11(a)–(g)). It is found that the k_{DC} value of CH_4 molecules in nanobubbles rises in the $MO_{Propanol}$ system at 0.09 and 1.24 μs (Fig. 4(a)). These dual surges in k_{DC} curve signify that CH_4 molecules have experienced two large diffusion fluctuations in the organoclay salt solution. The initial surge in k_{DC} curve finds its cause in the formation of CH_4 nanobubbles. A large number of CH_4 molecules in the solution aggregate to form spherical CH_4 nanobubbles, causing a CH_4 liquid to the gas phase transition (Fig. 3(a) and (b)). CH_4 molecules in nanobubbles diffuse faster than those in solution. The second surge in k_{DC} curve is attributed to the shape transformation of the CH_4 nanobubbles. A large number of CH_4 molecules enter the nanobubbles from the solution, and the shape of CH_4 nanobubbles changes from spherical shape to oval and finally to cylindrical shape (Figs. 3(g)–(h) and S9(a)–(d)). It is noted that the formation of this stable, system-spanning cylindrical nanobubble is likely due to the small size of the simulation system, i.e., the nanobubble could interact with its periodic image when growing to a size comparable to the dimensions of the simulation box. CH_4 molecules diffuse freely along the y-axis in the stable cylindrical nanobubble spanning the simulation box, and diffuse much faster than that in the spherical nanobubbles. Organic molecules may play a role in the shape change of CH_4 nanobubbles.

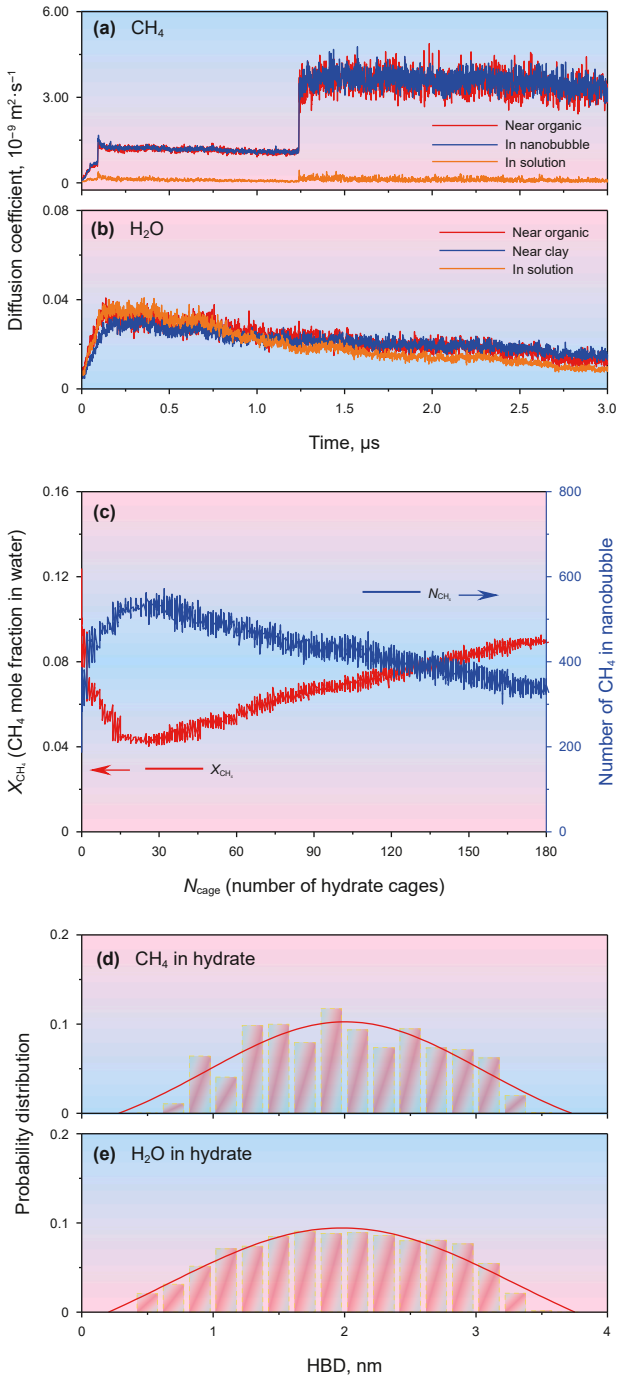

Fig. 4. Evolution of the diffusion coefficient (k_{DC}) for **(a)** CH_4 and **(b)** H_2O molecules in the $MO_{Propanol}$ system. **(c)** CH_4 mole fraction in water (x_{CH_4}) and the number of CH_4 in the nanobubbles (N_{CH_4}) under the hydrate cages (N_{cage}) (0–180) in the $MO_{Propanol}$ system. Probability distribution of the distance between hydrate (**(d)** CH_4 and **(e)** H_2O in hydrate and nanobubbles (HBD) in the $MO_{Butyric\text{-}acid}$ system over the last 0.05 μs.

The stable cylindrical nanobubble crosses the periodic boundary of the simulation box, thus CH_4 molecules could diffuse freely along *y* axis and diffuse much faster than those in the spherical nanobubbles. Therefore, the k_{DC} value after the second surge is more than twice that of the first (Fig. 4(a)). In particular, without organic molecules in the solution, the CH_4 molecules in the nanobubbles only experience the first surge in the system (Fig. S12(a)), while with the presence of organic molecules in the solution, two surges in k_{DC} curve occur in the system (Fig. S12(b)–(g)). The second surge in k_{DC} occurs at different times for different organic molecules (Fig. S12(b)–(g)). These findings indicate the pivotal role played by organic molecules in modulating the diffusion fluctuation of CH_4 molecules, primarily by controlling the size and shape of CH_4 nanobubbles. Furthermore, CH_4 molecules near organic molecules display comparable diffusion as CH_4 molecules in nanobubbles (Figs. 4(a) and S12(b)–(g)). This phenomenon arises from the fact that CH_4 molecules near organic molecules are contained in nanobubbles. Due to the position distribution of water molecules, all the H_2O molecules in the system are divided into three types, i.e., near organic molecules, near the clay surface, and in solution (Fig. S13(a)–(g)). The k_{DC} values of H_2O molecules first increase and then gradually decrease (Figs. 4(b) and S14(a)–(g)). Different organic molecules also have different numbers of CH_4 and H_2O molecules nearby (Fig. S15(a)–(b)).

On the other hand, previous MD studies have shown that the CH_4 and ion concentration in the solution are key factors controlling hydrate formation (Mi et al., 2022c). Organic molecules can affect the residence time of surrounding ions, which changes the local ion concentration and affects hydrate formation (Figs. 2(c) and S8(a)–(f)). In addition, the size of nanobubbles directly affects the CH_4 concentration in the solution (x_{CH_4}). The size of the nanobubbles is quantified by the number of CH_4 molecules in the nanobubbles (N_{CH_4}). As the hydrate cage (N_{cage}) forms, N_{CH_4} increases and x_{CH_4} decreases in the $MO_{Propanol}$ system (Fig. 4(c)). This phenomenon is attributed to the fact that in the early stages of the simulation, the spontaneous nucleation of CH_4 hydrate and the formation of nanobubbles are simultaneous and competitive, i.e., hydrate formation requires CH_4 molecules in the solution, while nanobubble formation also requires CH_4 molecules in the solution. As N_{cage} increases, N_{CH_4} decreases and x_{CH_4} increases, indicating that more CH_4 molecules are gradually transferred from the nanobubbles into the solution (Figs. 4(c) and S16(a)–(b)). The high CH_4 concentration promotes further formation of hydrate cages. If the simulation continues, the CH_4 nanobubbles continue to diminish in size until they eventually dissipate, and approximately 443 CH_4 hydrate cages form in the $MO_{Propanol}$ system (Fig. 4(c)). Furthermore, spontaneous nucleation of CH_4 hydrate occurs in the bulk solution away from the clay surfaces owing to the sharp decrease of x_{CH_4} in the clay interfacial region at the beginning of the simulation (Fig. S17(a)–(c)).

To reveal the pivotal role of CH_4 nanobubbles in the spontaneous nucleation of CH_4 hydrates, a comprehensive statistical analysis of the spatial relationship that exists between these nanobubbles and the hydrate solids is conducted. We define a parameter HBD, which is the distance between hydrates (comprising CH_4 and H_2O molecules) and nanobubbles. Interestingly, the probability distributions of HBD for CH_4 and H_2O molecules conform to a normal distribution with its peak occurring at 2.0 nm (Fig. 4(d) and (e)). This finding shows that CH_4 hydrates are primarily concentrated at a moderate distance away from the nanobubbles, with fewer hydrates located either close or further away from the nanobubbles. This finding is also observed in other systems (Fig. S18(a)–(g) and S19(a)–(g)). The number of CH_4 and H_2O molecules in hydrates under different HBD ranges (0.3–3.3 nm) in the $MO_{Butyric\text{-}acid}$ system is calculated, and the results are shown in Fig. 5(a) and (b). These values for the systems containing different organic molecules can be found in Fig. S20(a)–(g) and S21(a)–(g). It is found that in the early stage of simulation, HBD is mainly distributed near 2.0 nm, indicating that CH_4 hydrates are distributed in the region near 2.0 nm from the CH_4 nanobubbles (Fig. 5(a) and (b)). During the simulation process, CH_4 hydrates are gradually distributed in regions closer and farther from the CH_4 nanobubbles (Fig. 5(a) and (b)). The

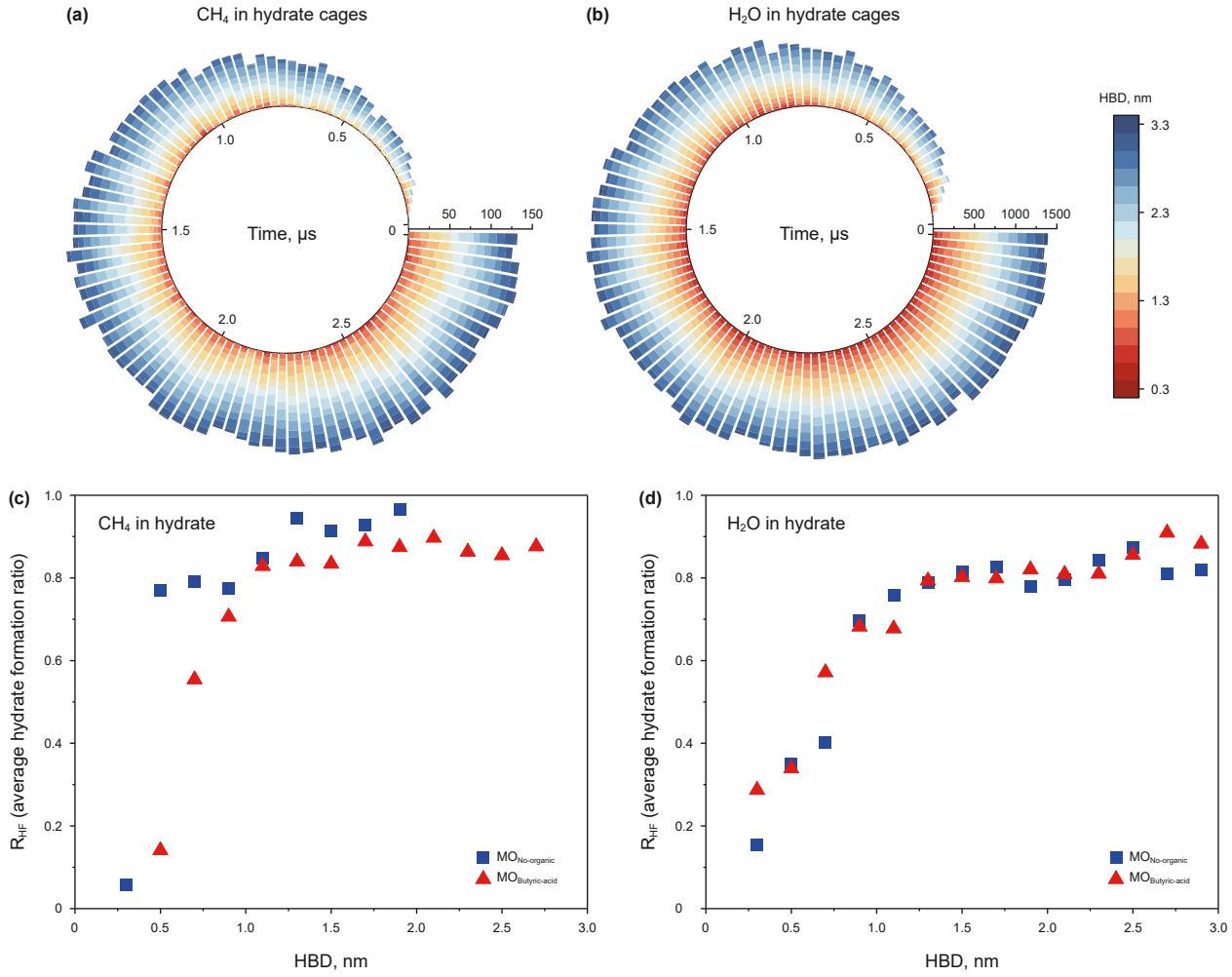

Fig. 5. Evolution of the number of **(a)** CH_4 and **(b)** H_2O in hydrate cages along the distance between hydrate and nanobubbles (HBD) in the $MO_{Butyric\text{-}acid}$ system. Average hydrate formation ratio (R_{HF}) of **(c)** CH_4 and **(d)** H_2O molecules in hydrate cages in the HBD ranges (0–3.0 nm) for the $MO_{No\text{-}organic}$ and $MO_{Butyric\text{-}acid}$ systems at 2.0 μs. The R_{HF} is defined as the time duration during which the CH_4 or H_2O molecule retains its hydrate state in subsequent simulations divided by the total subsequent time.

majority of CH_4 hydrates tend to be situated within the 1–3 nm ranges from the CH_4 nanobubbles (Fig. 5(a) and (b)). At the end of the simulation, a few CH_4 hydrates are observed within regions that are either within 1 nm of the nanobubbles or more than 3 nm away from them (Fig. 5(a) and (b)). To assess the stability of spontaneous nucleation of CH_4 hydrates in different HBD values, we define the hydrate formation ratio (R_{HF}). This metric gauges whether a hydrate (comprising CH_4 and H_2O molecules) will maintain its hydrate state or transition into another state over the course of subsequent simulations. R_{HF} is calculated as the time during which the CH_4 or H_2O molecule retains its hydrate state in subsequent simulations divided by the total subsequent time. R_{HF} of CH_4 and H_2O molecules in hydrates for the $MO_{No\text{-}organic}$ and $MO_{Butyric\text{-}acid}$ systems at 2 μs is counted, and the results are shown in Fig. 5(c) and (d). With the increase in HBD values, R_{HF} values first gradually increase (Fig. 5(c) and (d)). Beyond an HBD of 1.0 nm, the R_{HF} values for CH_4 and H_2O molecules stabilize at approximately 0.9 and 0.8, respectively (Fig. 5(c) and (d)). This finding indicates that in the region 1.0 nm away from the CH_4 nanobubbles, the closer the CH_4 hydrate is to the nanobubbles, the more unstable it is; in the region above 1.0 nm away from the CH_4 nanobubbles, CH_4 hydrates are not easily dissociated, showing high stability.

3.3. *Effect of organic molecules on CH_4 hydrate nucleation from organoclay salt solution*

Different organic molecules exert distinct effects on the spontaneous nucleation of CH_4 hydrates. We analyzed the time distribution of CH_4 molecules (which form hydrates at 1.0 μs) in the nanobubble and near organic molecules during the simulation period of 0–1.0 μs (Fig. 6(a)–(f)). It is observed that the highest density area appears in the lower left corner of the Fig. for the six systems, i.e., a large number of CH_4 molecules are near the nanobubbles and organic molecules for a short time (Fig. 6(a)–(f)). This shows that the CH_4 molecules that form hydrates at 1.0 μs are in the solution for a long time, which also confirms that CH_4 molecules in the solution are more likely to form CH_4 hydrates. In addition, in the $MO_{Butyric\text{-}acid}$, $MO_{Propylamine}$, $MO_{Propanol}$, and MO_{Butane} systems, a high-density area appears below the Figure, indicating that CH_4 molecules spend longer periods in the nanobubbles than near organic molecules (Fig. 6(a)–(c) and (e)). In the $MO_{Pentene}$ and $MO_{Phenylpropane}$ systems, a high-density area approaches the median line, which is related to the number of CH_4 molecules near the organic molecules (Figs. 6(d)–(e) and S11(a)–(g)). Notably, in the $MO_{Propanol}$ system, the density in the red circle is larger than that in other systems, indicating that a

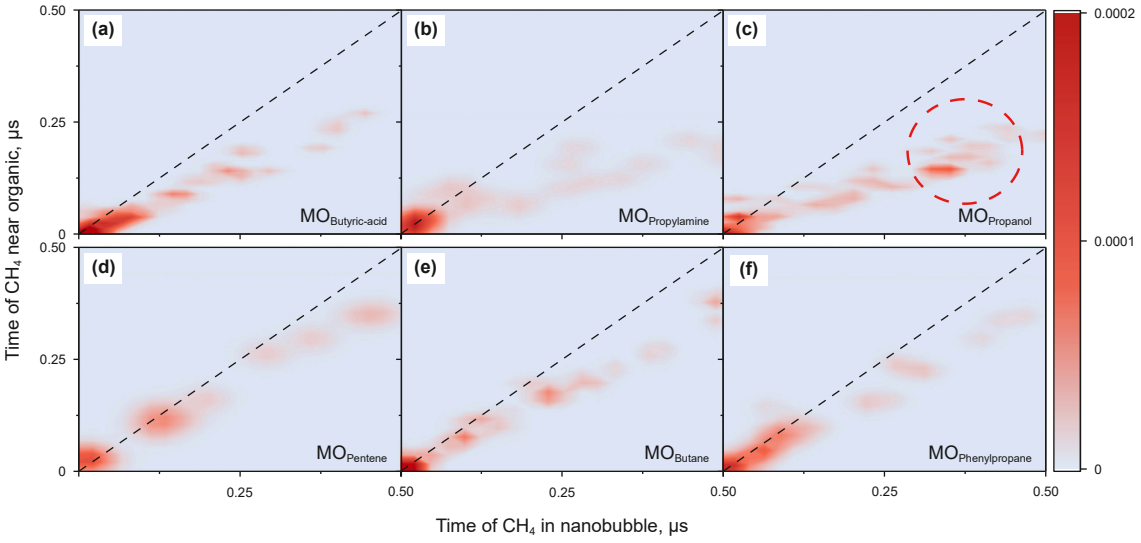

Fig. 6. The time distribution of CH_4 molecules (which form hydrate cages at 1.0 μs) in the nanobubble and near organic molecules during the simulation period of 0–1.0 μs in the six systems i.e., **(a)** $MO_{Butyric\text{-}acid}$, **(b)** $MO_{Propylamine}$, **(c)** $MO_{Propanol}$, **(d)** $MO_{Pentene}$, **(e)** MO_{Butane} and **(f)** $MO_{Phenylpropane}$.

greater number of CH_4 molecules in the nanobubbles transition into the hydrate. This trend underscores that propanol molecules adsorbed to the CH_4 nanobubble surface promote CH_4 hydrate nucleation, exhibiting a distinct advantage over other organic molecules.

The F_4 order parameters and hydrate formation rates for the seven systems are shown in Fig. 7(a) and (b). The hydrate formation rate, which quantifies the number of hydrate cages generated per microsecond, offers a reliable metric for evaluating the effect of different organic molecules on the spontaneous nucleation of CH_4 hydrate. At the end of the simulation, the F_4 and the number of cages of the $MO_{Propanol}$ system are the highest, followed by the MO_{Butane} and $MO_{No\text{-}organic}$ systems (Figs. 7(a) and S22). Additionally, the hydrate formation rates for these three systems are 55, 56, and 42, respectively (Fig. 7(b)). Propanol is known to be a thermodynamic inhibitor of hydrate formation. However, our observations show that propanol can kinetically promote the spontaneous nucleation of CH_4 hydrates in oceanic sediments. These observations indicate that propanol and butane molecules kinetically promote the spontaneous nucleation of CH_4 hydrate from organoclay salt solutions. However, propanol and butane molecules employ different mechanisms to enhance CH_4 hydrate nucleation. For propanol molecules, their promoting ability surpasses their inhibiting ability. Specifically, although hydrophilic propanol molecules inhibit the spontaneous nucleation of CH_4 hydrate by forming hydrogen bonds with H_2O molecules, propanol molecules strongly bind surrounding H_2O molecules and repel CH_4 molecules in the early stages of the simulation, increasing the local CH_4 concentration and promoting hydrate formation (Fig. 2(c)). Moreover, propanol molecules can suppress the fluctuations of surrounding ions and delay the nanobubble transition from spherical to cylindrical in shape (Figs. 2(c) and 4(a)). Not only that, propanol molecules facilitate the transfer of CH_4 molecules from the nanobubbles into the hydrates (Fig. 6(c)). In contrast, butane molecules display miscibility with CH_4 molecules, and can serve as guest molecules to form butane hydrates (Figs. S6(d), S23 and S24(a)–(b)). Cage-like structures around the butane molecules adsorbed on the nanobubble surface (Fig. S24(c)). This suggests that the spontaneous nucleation of butane/CH_4 mixed hydrates is more accessible than that of pure CH_4 hydrate. The F_4 values and

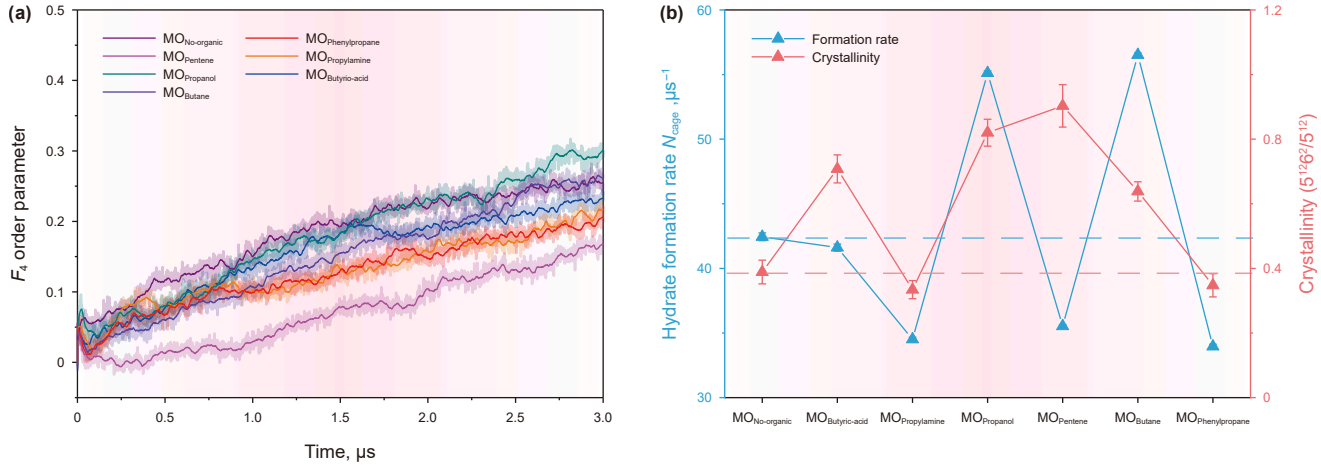

Fig. 7. Evolution of **(a)** F_4 order parameter for water molecules in seven systems. **(b)** Hydrate formation rate and crystallinity over the last 0.1 μs in seven systems i.e., $MO_{No\text{-}organic}$, $MO_{Butyric\text{-}acid}$, $MO_{Propylamine}$, $MO_{Propanol}$, $MO_{Pentene}$, MO_{Butane}, and $MO_{Phenylpropane}$.

hydrate formation rates in the $MO_{Butyric\text{-}acid}$, $MO_{Propylamine}$, and $MO_{Phenylpropane}$ systems are marginally lower than those in the $MO_{No\text{-}organic}$ system (Fig. 7(a) and (b)), indicating that butyric-acid, propylamine and phenylpropane molecules exhibit a slight inhibitory effect on spontaneous nucleation of CH_4 hydrates from organoclay salt solutions. This may be due to the strong interaction between butyric-acid and propylamine molecules and H_2O molecules in the solution inhibiting the spontaneous nucleation of CH_4 hydrates. The adsorption of CH_4 nanobubbles by the benzene ring in the phenylpropane molecule inhibits the transition of CH_4 molecules from nanobubbles to hydrates (Fig. S6(f) and S10(g)), in line with previous MD studies (Fengyi et al., 2023). In particular, the F_4 value of the $MO_{Pentene}$ system is much lower than that of the other systems, and the hydrate formation rate of the $MO_{Pentene}$ system is only around 35, indicating that the pentene molecule exhibits a strong inhibitory ability to spontaneous nucleation of CH_4 hydrates (Fig. 7(a) and (b)). Pentene molecules cannot act as guest molecules for hydrates and are miscible with CH_4 molecules (Fig. S6(d)), which provides a new perspective for the development of new hydrate inhibitors. Interestingly, although 5^{12} and $5^{12}6^2$ cages constitute the majority of hydrate structures (Fig. S25(a)–(g)), organic molecules do not significantly reduce the crystallinity, and may even enhance it (Figs. 7(b) and S26). This may be related to the stochastic nature of the spontaneous nucleation of CH_4 hydrate and the arrangement of organic molecules to surrounding H_2O molecules. For propanol molecules, their promoting ability for hydrate formation surpasses their inhibiting ability, which can be explained by a “balanced interaction” mechanism. A key distinction lies in the different hydrophilic functional groups of these organic molecules: the carboxyl group (–COOH) of butyric acid and the amino group ($–NH_2$) of propylamine have more hydrogen bond donors and hydrogen bond acceptors than the hydroxyl group (–OH) of propanol. Consequently, butyric acid and propylamine could interact more strongly with their surrounding water molecules by forming more hydrogen bonds, and make these water molecules have configurations incompatible with clathrate cages, thus kinetically hindering their reorientation required for hydrate nucleation. This explains their slight inhibitory effect seen in Fig. 7(a).

Furthermore, the slight inhibitory effects observed for butyric acid and propylamine are in excellent agreement with some experimental studies on amino acids and carboxylic acids as kinetic hydrate inhibitors (KHIs) (Bavoh et al., 2019). These molecules are known to delay nucleation, and our simulations attribute this to their strong, rigid hydrogen bonding with water, which kinetically hinders the formation of clathrate cage structures. The observation that clay surfaces and organic molecules can work in concert to influence nucleation kinetics aligns well with recent experimental results on the synergistic promotion by clay-organic systems (Liu et al., 2023a; Zhao et al., 2021), for which we now provide a foundational molecular mechanism.

3.4. The dual role of propanol as a kinetic promoter and thermodynamic inhibitor

A key finding of this study is the pronounced kinetic promotion of CH_4 hydrate nucleation by propanol, which warrants a deeper mechanistic explanation, especially given its established role as a thermodynamic inhibitor. This apparent contradiction is resolved by distinguishing its bulk effects from its localized kinetic role at the interface of nanobubbles, which is the primary site for hydrate nucleation. In the bulk aqueous phase, propanol competes with water–water hydrogen bonding, disrupting the water structure required for the highly ordered clathrate lattice. This bulk effect is the basis of its function as a thermodynamic inhibitor. However, this simulation study reveals that the crucial promoting effect occurs not in the bulk solution but at the interface of CH_4–water, where propanol molecules preferentially adsorb. At this specific location, their 'balanced' hydrogen bonding does not simply disrupt; it pre-organizes the interfacial water molecules into a state structurally more amenable to forming clathrate cages. Propanol may effectively act as a template or a heterogeneous nucleation site, facilitating the formation of cage-like water motifs around the guest CH_4 molecules. This templating effect lowers the kinetic activation energy barrier for forming a critical hydrate nucleus. The process of hydrate nucleation is governed by the specific molecular events at the most favorable site, not by the average properties of the bulk solution. Therefore, the competitive balance between inhibition and promotion of propanol is dictated at the interface. While the inhibitory effect of propanol is a diffuse, bulk thermodynamic property, its promotional effect is a potent, localized kinetic phenomenon concentrated exactly where nucleation begins. At the nucleation stage of CH_4 hydrate, this promoting effect dominates the process, accelerating the hydrate formation rate.

4. Conclusions

Microsecond MD simulations are performed to investigate the spontaneous nucleation of CH_4 hydrates in oceanic sediments, to reveal the effects of representative small organic molecules (such as butane, propanol, phenylpropane, pentene, butyric-acid, and propylamine). The simulation results indicate that the spontaneous nucleation of CH_4 hydrates is influenced by a coupling of organic molecules, clay surfaces and salt ions, where organic molecules alter the spontaneous nucleation of CH_4 hydrates by modulating the diffusion fluctuations of CH_4 molecule via controlling the shape and size of CH_4 nanobubbles. Organic molecules may promote the shape transformation of CH_4 nanobubbles from spherical to cylindrical. CH_4 molecules have experienced two large diffusion fluctuations in the organoclay salt solution, i.e., the formation and shape transformation of CH_4 nanobubbles from spherical to cylindrical. All organic molecules are mainly distributed inside or on the surface of CH_4 nanobubbles to modulate the diffusion fluctuation of CH_4 molecules. Furthermore, the probability distributions of the distance between hydrates and nanobubbles conform to a normal distribution, i.e., CH_4 hydrates are primarily concentrated at a moderate distance away from the nanobubbles, with a lesser number of hydrates located either close or at a more distant remove from the nanobubbles. On the other hand, in the region 1.0 nm away from the CH_4 nanobubbles, the closer the CH_4 hydrate is to the nanobubbles, the more unstable it is; in the region higher from 1.0 nm away from the CH_4 nanobubbles, CH_4 hydrates are not easily dissociated and show high stability.

Different organic molecules exert distinct effects on the spontaneous nucleation of CH_4 hydrates. Specifically, propanol molecules adsorbed to the CH_4 nanobubble surface kinetically promote CH_4 hydrate nucleation, exhibiting a distinct advantage over other organic molecules; the spontaneous nucleation of butane/CH_4 mixed hydrate is more accessible than that of pure CH_4 hydrate; butyric-acid, propylamine, phenylpropane and pentene molecules exhibit an inhibitory effect on spontaneous nucleation of CH_4 hydrates from organoclay salt solutions. These molecular insights can help to understand the formation of natural gas hydrate resources and effectively utilize this resource. This preliminary study into the microscopic mechanism of the effect of organic molecules on spontaneous hydrate nucleation can help to understand the formation of natural gas hydrate resources, and will catalyze more inventive research, particularly with regard to CH_4 hydrate

exploitation, hydrate-based CO_2 sequestration and seawater desalination.

The results and mechanisms presented herein are derived from MD simulations using an idealized slit nanopore model with a single mineral type (montmorillonite) and representative small organic molecules. Natural marine sediments are vastly more complex, featuring a wide distribution of pore sizes and heterogeneous architectures, diverse mineralogies, and a complex mixture of organic matter. The value of this study does not lie in providing a comprehensive field-scale prediction, but in elucidating the fundamental, molecular-level mechanisms (such as the role of nanobubble morphology and the dual kinetic/thermodynamic nature of inhibitors) that form the essential foundation of these larger, more complex geological processes. These molecular insights provide a basis for the phenomena observed at the macroscale and can help guide the development of future multi–scale models.

CRediT authorship contribution statement

Feng-Yi Mi: Writing – original draft, Visualization, Validation, Methodology, Investigation, Formal analysis, Data curation. **Zhong-Jin He:** Writing – review & editing, Supervision, Project administration, Funding acquisition, Formal analysis, Conceptualization. **Jiang-Tao Pang:** Writing – review & editing. **Othonas A. Moultos:** Writing – review & editing, Resources. **Thijs J.H. Vlugt:** Writing – review & editing, Resources. **Guo-Sheng Jiang:** Writing – review & editing. **Fu-Long Ning:** Writing – review & editing, Resources, Funding acquisition.

Declaration of competing interest

The authors declare that they have no known competing financial interests or personal relationships that could have appeared to influence the work reported in this paper.

Acknowledgements

This work was supported by the National Natural Science Foundation of China (Nos. 42376202, 41976203), National Science Foundation for Distinguished Young Scholars (42225207), Natural Science Foundation of Hubei Province (2021CFA024), and China Scholarship Council (CSC202306410133).

Supplementary data

Supplementary data to this article can be found online at https://doi.org/10.1016/j.petsci.2026.02.012.

References

Abascal, J.L., Sanz, E., Garcia Fernandez, R., et al., 2005. A potential model for the study of ices and amorphous water: TIP4P/Ice. J. Chem. Phys. 122, 234511. https://doi.org/10.1063/1.1931662.

Bavoh, C.B., Lal, B., Osei, H., et al., 2019. A review on the role of amino acids in gas hydrate inhibition, CO_2 capture and sequestration, and natural gas storage. J. Nat. Gas Sci. Eng. 64, 52–71. https://doi.org/10.1016/j.jngse.2019.01.020.

Berendsen, H.J.C., Postma, J.P.M., Vangunsteren, W.F., et al., 1984. Molecular-dynamics with coupling to an external Bath. J. Chem. Phys. 81, 3684–3690. https://doi.org/10.1063/1.448118.

Boswell, R., 2009. Engineering. Is gas hydrate energy within reach? Science 325, 957–958. https://doi.org/10.1126/science.1175074.

Bussi, G., Donadio, D., Parrinello, M., 2007. Canonical sampling through velocity rescaling. J. Chem. Phys. 126, 014101. https://doi.org/10.1063/1.2408420.

Chen, Y., Takeya, S., Sum, A.K., 2023. Topological dual and extended relations between networks of clathrate hydrates and Frank-Kasper phases. Nat. Commun. 14, 596. https://doi.org/10.1038/s41467-023-36242-4.

Collett, T.S., Lee, M.W., Agena, W.F., et al., 2011. Permafrost-associated natural gas hydrate occurrences on the Alaska North Slope. Mar. Petrol. Geol. 28, 279–294. https://doi.org/10.1016/j.marpetgeo.2009.12.001.

Cygan, R.T., Liang, J.J., Kalinichev, A.G., 2004. Molecular models of hydroxide, oxyhydroxide, and clay phases and the development of a general force field. J. Phys. Chem. B 108, 1255–1266. https://doi.org/10.1021/jp0363287.

Darden, T., York, D., Pedersen, L., 1993. Particle mesh Ewald: an N·log(N) method for Ewald sums in large systems. J. Chem. Phys. 98, 10089–10092. https://doi.org/10.1063/1.464397.

Downs, R.T., Hall-Wallace, M., 2003. The crystal structure database. Am. Mineral. 88, 247–250.

Fang, B., Lü, T., Li, W., et al., 2024. Microscopic insights into poly-and mono-crystalline methane hydrate dissociation in Na-montmorillonite pores at static and dynamic fluid conditions. Energy 288, 129755. https://doi.org/10.1016/j.energy.2023.129755.

Fengyi, M., Zhongjin, H., Guosheng, J., et al., 2023. Molecular insights into the effects of lignin on methane hydrate formation in clay nanopores. Energy 276, 127496. https://doi.org/10.1016/j.energy.2023.127496.

Haq, B.U., 1999. Natural gas deposits - methane in the deep blue sea. Science 285, 543–544. https://doi.org/10.1126/science.285.5427.543.

He, Z., Ning, F., Mi, F., et al., 2022. Molecular dynamics study on the spontaneous adsorption of aromatic carboxylic acids to methane hydrate surfaces: implications for hydrate antiagglomeration. Energy Fuels 36, 3628–3639. https://doi.org/10.1021/acs.energyfuels.2c00347.

Hess, B., Kutzner, C., van der Spoel, D., et al., 2008. GROMACS 4: algorithms for highly efficient, load-balanced, and scalable molecular simulation. J. Chem. Theor. Comput. 4, 435–447. https://doi.org/10.1021/ct700301q.

Huang, X., Zhu, Y.-J., Wang, X.-H., et al., 2024. The development of high-performance kinetic hydrate inhibitors by introducing N-vinyl caprolactam and vinyl ether homopolymers into PVCap. Pet. Sci. 21, 4454–4463. https://doi.org/10.1016/j.petsci.2024.09.001.

Ji, H., Chen, D., Zhao, C., et al., 2018. Molecular dynamics simulation of methane hydrate formation and dissociation in the clay pores with fatty acids. J. Phys. Chem. C 122, 1318–1325. https://doi.org/10.1021/acs.jpcc.7b08808.

Ji, H.Q., Wu, G.Z., Zi, M.C., et al., 2016. Microsecond molecular dynamics simulation of methane hydrate formation in humic-acid-amended sodium montmorillonite. Energy Fuels 30, 7206–7213. https://doi.org/10.1021/acs.energyfuels.6b01544.

Jia, Y.X., Zhao, Y., Li, M., et al., 2022. Biodegradable organics as a multisystem-compatible low-dose green kinetic hydrate inhibitor. ACS Sustain. Chem. Eng. 10, 11320–11329. https://doi.org/10.1021/acssuschemeng.2c03342.

Jorgensen, W.L., Madura, J.D., Swenson, C.J., 1984. Optimized intermolecular potential functions for liquid hydrocarbons. J. Am. Chem. Soc. 106, 6638–6646. https://doi.org/10.1021/ja00334a030.

Jorgensen, W.L., Maxwell, D.S., TiradoRives, J., 1996. Development and testing of the OPLS all-atom force field on conformational energetics and properties of organic liquids. J. Am. Chem. Soc. 118, 11225–11236. https://doi.org/10.1021/ja9621760.

Kelleher, B.P., Simpson, A.J., Rogers, R.E., et al., 2007. Effects of natural organic matter from sediments on the growth of marine gas hydrates. Mar. Chem. 103, 237–249. https://doi.org/10.1016/j.marchem.2006.09.002.

Koh, C.A., 2002. Towards a fundamental understanding of natural gas hydrates. Chem. Soc. Rev. 31, 157–167. https://doi.org/10.1039/b008672j.

Konno, Y., Fujii, T., Sato, A., et al., 2017. Key findings of the world's first offshore methane hydrate production test off the Coast of Japan: toward future commercial production. Energy Fuels 31, 2607–2616. https://doi.org/10.1021/acs.energyfuels.6b03143.

Kvenvolden, K.A., 1993. Gas hydrates - geological perspective and global change. Rev. Geophys. 31, 173–187. https://doi.org/10.1029/93rg00268.

Kvenvolden, K.A., 1995. A review of the geochemistry of methane in natural gas hydrate. Org. Geochem. 23, 997–1008. https://doi.org/10.1016/0146-6380(96)00002-2.

Kyung, D., Lim, H.-K., Kim, H., et al., 2015. CO_2 hydrate nucleation kinetics enhanced by an organo-mineral complex formed at the montmorillonite-water interface. Environ. Sci. Technol. 49, 1197–1205. https://doi.org/10.1021/es504450x.

Lamorena, R.B., Kyung, D., Lee, W., 2011. Effect of organic matters on CO_2 hydrate formation in Ulleung basin sediment suspensions. Environ. Sci. Technol. 45, 6196–6203. https://doi.org/10.1021/es201261y.

Li, J., Ye, J., Qin, X., et al., 2018. The first offshore natural gas hydrate production test in South China Sea. China Geol. 1, 5–16. https://doi.org/10.31035/cg2018003.

Li, X.S., Xu, C.G., Zhang, Y., et al., 2016. Investigation into gas production from natural gas hydrate: a review. Appl. Energy 172, 286–322. https://doi.org/10.1016/j.apenergy.2016.03.101.

Li, Y., Chen, M., Tang, H., et al., 2022. Insights into carbon dioxide hydrate nucleation on the external basal surface of clay minerals from molecular dynamics simulations. ACS Sustain. Chem. Eng. 10, 6358–6369. https://doi.org/10.1021/acssuschemeng.2c01046.

Liao, B., Wang, J.T., Sun, J.S., et al., 2023. Microscopic insights into synergism effect of different hydrate inhibitors on methane hydrate formation: experiments and molecular dynamics simulations. Fuel 340, 127488. https://doi.org/10.1016/j.fuel.2023.127488.

Liu, H., Shi, C., Wang, S., et al., 2023a. Clay nanoflakes and organic molecules synergistically promoting CO_2 hydrate formation. J. Colloid Interface Sci. 641, 812–819. https://doi.org/10.1016/j.jcis.2023.03.118.

Liu, H.Q., Shi, C.R., Chen, Z.R., et al., 2023b. Turning gas hydrate nucleation with oxygen-containing groups on size- selected graphene oxide flakes. J. Energy Chem. 87, 351–358. https://doi.org/10.1016/j.jechem.2023.08.029.

Liu, Y., Zhang, L., Yang, L., et al., 2021a. Behaviors of CO_2 hydrate formation in the presence of acid-dissolvable organic matters. Environ. Sci. Technol. 55, 6206–6213. https://doi.org/10.1021/acs.est.0c06407.

Liu, Y.Z., Feng, Y., Zhang, L.X., et al., 2021b. Effects of protein macromolecules and metabolic small molecules on kinetics of methane hydrate formation in marine clay. Chem. Eng. J. 412, 128496. https://doi.org/10.1016/j.cej.2021.128496.

Liu, Y.Z., Feng, Y., Zhao, Y., et al., 2021c. Self-organized colloids thermodynamically weaken the effect of salt on methane hydrate formation. ACS Sustain. Chem. Eng. 9, 11323–11330. https://doi.org/10.1021/acssuschemeng.1c02179.

Liu, Z., Zheng, J.J., Wang, Z.Y., et al., 2023c. Effect of clay on methane hydrate formation and dissociation in sediment: implications for energy recovery from clayey-sandy hydrate reservoirs. Appl. Energy 341, 121064. https://doi.org/10.1016/j.apenergy.2023.121064.

Makogon, Y.F., Holditch, S.A., Makogon, T.Y., 2007. Natural gas-hydrates - a potential energy source for the 21st century. J. Petrol. Sci. Eng. 56, 14–31. https://doi.org/10.1016/j.petrol.2005.10.009.

Mi, F., He, Z., Fang, B., et al., 2022a. Molecular insights into the effects of surface property and pore size of non-swelling clay on methane hydrate formation. Fuel 311, 122607. https://doi.org/10.1016/j.fuel.2021.122607.

Mi, F., He, Z., Jiang, G., et al., 2022b. Effects of marine environments on methane hydrate formation in clay nanopores: a molecular dynamics study. Sci. Total Environ. 852, 158454. https://doi.org/10.1016/j.scitotenv.2022.158454.

Mi, F., He, Z., Jiang, G., et al., 2024a. Effect of glucose on CH_4 hydrate formation in clay nanopores and bulk solution: insights from microsecond molecular dynamics simulations. ACS Sustain. Chem. Eng. 12, 4644–4654. https://doi.org/10.1021/acssuschemeng.3c08280.

Mi, F., He, Z., Jiang, G., et al., 2024b. What roles do interlayer cations (K^+) and salt ions (Na^+ and Cl^-) play in methane hydrate formation in illite nanopore? Appl. Clay Sci. 256, 107428. https://doi.org/10.1016/j.clay.2024.107428.

Mi, F., He, Z., Ning, F., 2025a. Molecular dynamics simulation on CO_2 hydrate growth and CH_4-CO_2 replacement in various clay nanopores. Energy 314, 134282. https://doi.org/10.1016/j.energy.2024.134282.

Mi, F., He, Z., Ning, F., 2025b. Molecular insight on CO_2/C_3H_8 mixed hydrate formation from the brine for sustainable hydrate-based desalination. Sep. Purif. Technol. 353, 128244. https://doi.org/10.1016/j.seppur.2024.128244.

Mi, F., He, Z., Pang, J., et al., 2024c. Molecular insights into hybrid CH_4 physisorption-hydrate formation in spiral halloysite nanotubes: implications for energy storage. ACS Appl. Mater. Interfaces 16, 67587–67596. https://doi.org/10.1021/acsami.4c11288.

Mi, F., He, Z., Zhao, Y., et al., 2022c. Effects of surface property of mixed clays on methane hydrate formation in nanopores: a molecular dynamics study. J. Colloid Interface Sci. 627, 681–691. https://doi.org/10.1016/j.jcis.2022.07.101.

Mi, F., Li, W., Pang, J., et al., 2024d. Molecular insights into the microscopic behavior of CO_2 hydrates in Oceanic sediments: implications for carbon sequestration. J. Phys. Chem. C 128, 18588–18597. https://doi.org/10.1021/acs.jpcc.4c05413.

Mi, F.Y., He, Z.J., Cheng, L.W., et al., 2023. Molecular dynamics simulation on methane hydrate formation in clay nanopores of edge surfaces. Appl. Clay Sci. 243, 107069. https://doi.org/10.1016/j.clay.2023.107069.

Milkov, A.V., 2004. Global estimates of hydrate-bound gas in marine sediments: how much is really out there? Earth Sci. Rev. 66, 183–197. https://doi.org/10.1016/j.earscirev.2003.11.002.

Ning, F., Yu, Y., Kjelstrup, S., et al., 2012. Mechanical properties of clathrate hydrates: status and perspectives. Energy Environ. Sci. 5, 6779–6795. https://doi.org/10.1039/c2ee03435b.

Nosé, S., 1984. A molecular-dynamics method for simulations in the canonical ensemble. Mol. Phys. 52, 255–268. https://doi.org/10.1080/00268978400101201.

Park, T., Kyung, D., Lee, W., 2014. Effect of organic matter on CO_2 hydrate phase equilibrium in phyllosilicate suspensions. Environ. Sci. Technol. 48, 6597–6603. https://doi.org/10.1021/es405099z.

Parrinello, M., Rahman, A., 1980. Crystal-structure and pair potentials - a molecular-dynamics study. Phys. Rev. Lett. 45, 1196–1199. https://doi.org/10.1103/PhysRevLett.45.1196.

Qin, Y., Shang, L.Y., Lv, Z.B., et al., 2022. Methane hydrate formation in porous media: overview and perspectives. J. Energy Chem. 74, 454–480. https://doi.org/10.1016/j.jechem.2022.07.019.

Ren, J., Liu, X., Niu, M., et al., 2022. Effect of sodium montmorillonite clay on the kinetics of CH_4 hydrate - implication for energy recovery. Chem. Eng. J. 437, 135368. https://doi.org/10.1016/j.cej.2022.135368.

Ren, J.J., Zeng, S.Y., Chen, D.Y., et al., 2023. Roles of montmorillonite clay on the kinetics and morphology of CO_2 hydrate in hydrate-based CO_2 sequestration. Appl. Energy 340, 120997. https://doi.org/10.1016/j.apenergy.2023.120997.

Saito, H., Suzuki, N., 2007. Terrestrial organic matter controlling gas hydrate formation in the Nankai trough accretionary prism, offshore Shikoku, Japan. J. Geochem. Explor. 95, 88–100. https://doi.org/10.1016/j.gexplo.2007.05.007.

Sloan Jr., E.D., 2003. Fundamental principles and applications of natural gas hydrates. Nature 426, 353–363. https://doi.org/10.1038/nature02135.

Sloan ED, K.C., 2008. Clathrate Hydrates of Natural Gases, third ed. CRC Press, Boca Raton, FL.

Wallmann, K., Aloisi, G., Haeckel, M., et al., 2006. Kinetics of organic matter degradation, microbial methane generation, and gas hydrate formation in anoxic marine sediments. Geochim. Cosmochim. Acta 70, 3905–3927. https://doi.org/10.1016/j.gca.2006.06.003.

Walsh, M.R., Koh, C.A., Sloan, E.D., et al., 2009. Microsecond simulations of spontaneous methane hydrate nucleation and growth. Science 326, 1095–1098. https://doi.org/10.1126/science.1174010.

Wang, R., Liu, T.L., Ning, F.L., et al., 2019. Effect of hydrophilic silica nanoparticles on hydrate formation: insight from the experimental study. J. Energy Chem. 30, 90–100. https://doi.org/10.1016/j.jechem.2018.02.021.

Wang, X., Yuan, Y., Du, Z., et al., 2025. Study on the effect of clay minerals on phase transition of methane hydrate in sand sediments: kinetic behavior and microstructural observation. Pet. Sci. 22, 3029–3041. https://doi.org/10.1016/j.petsci.2025.03.047.

Xu, P., Lang, X.M., Fan, S.S., et al., 2016. Molecular dynamics simulation of methane hydrate growth in the presence of the natural product pectin. J. Phys. Chem. C 120, 5392–5397. https://doi.org/10.1021/acs.jpcc.5b10342.

Yan, K.-F., Zhao, J.-Y., Chen, H., et al., 2023. Exploring hydration mechanism of salt ions on the methane hydrate formation: insights from experiments, QM calculations and MD simulations. Chem. Eng. Sci. 276, 118829. https://doi.org/10.1016/j.ces.2023.118829.

Yun, S., Jo, I., Go, W., et al., 2023. Water-soluble cellulose as a new class of green CH_4 hydrate inhibitors: insights from experiments and molecular dynamics simulations. ACS Sustain. Chem. Eng. 11, 6153–6162. https://doi.org/10.1021/acssuschemeng.2c06242.

Zeng, H., Wilson, L.D., Walker, V.K., et al., 2006. Effect of antifreeze proteins on the nucleation, growth, and the memory effect during tetrahydrofuran clathrate hydrate formation. J. Am. Chem. Soc. 128, 2844–2850. https://doi.org/10.1021/ja0548182.

Zhang, C.L., Pancost, R.D., Sassen, R., et al., 2003. Archaeal lipid biomarkers and isotopic evidence of anaerobic methane oxidation associated with gas hydrates in the Gulf of Mexico. Org. Geochem. 34, 827–836. https://doi.org/10.1016/S0146-6380(03)00003-2.

Zhang, J., Fu, H.-Q., Guo, M.-Z., et al., 2024. New insights into the deposition of natural gas hydrate on pipeline surfaces: a molecular dynamics simulation study. Pet. Sci. 21, 694–704. https://doi.org/10.1016/j.petsci.2023.08.027.

Zhang, Z., Kusalik, P.G., Wu, N., et al., 2022. Molecular insights into the impacts of calcite nanoparticles on methane hydrate formation. ACS Sustain. Chem. Eng. 10, 11597–11605. https://doi.org/10.1021/acssuschemeng.2c03428.

Zhang, Z., Liu, L.L., Lu, W.J., et al., 2023. Permeability of hydrate-bearing fine-grained sediments: research status, challenges and perspectives. Earth Sci. Rev. 244, 104517. https://doi.org/10.1016/j.earscirev.2023.104517.

Zhao, J., Liu, Y., Yang, L., et al., 2021. Organics-coated nanoclays further promote hydrate formation kinetics. J. Phys. Chem. Lett. 12, 3464–3467. https://doi.org/10.1021/acs.jpclett.1c00010.

Zhu, Y.-J., Yang, X.-M., Huang, X., et al., 2024. Acoustic characterization of hydrate formation and decomposition in clay-bearing sediments. Pet. Sci. 21, 2830–2838. https://doi.org/10.1016/j.petsci.2024.06.008.